Redox Behaviour of the Iron–Sulphur Cluster $[Fe_6(\mu_3\text{-}S)_8(PEt_3)_6]^{2+}$. Synthesis and Crystal Structure of the New Paramagnetic Monopositive Species $[Fe_6(\mu_3\text{-}S)_8(PEt_3)_6]^+$ as its $[PF_6]^-$ Salt†

Franco Cecconi, Carlo A. Ghilardi, Stefano Midollini, and Annabella Orlandini *
Istituto per lo Studio della Stereochimica ed Energetica dei Composti di Coordinazione, C.N.R., Via F. D. Guerrazzi, 27, 50132 Firenze, Italy
Piero Zanello
Dipartimento di Chimica, Università di Siena, Pian dei Mantellini, 44, 53100 Siena, Italy

---

The electrochemical behaviour of the complex cation $[Fe_6(\mu_3\text{-}S)_8(PEt_3)_6]^{2+}$ in non-aqueous solvents demonstrates the ability of the Fe_6S_8 core to undergo, through well defined steps, the one-electron transfer series: $[Fe_6S_8]^{4+} \rightleftarrows [Fe_6S_8]^{3+} \rightleftarrows [Fe_6S_8]^{2+} \rightleftarrows [Fe_6S_8]^+ \rightleftarrows [Fe_6S_8]^0$. Attempts to obtain some congeners of $[Fe_6S_8(PEt_3)_6]^{2+}$ either by electrochemical techniques or by common redox agents proved to be unsuccessful. However, the monopositive species $[Fe_6(\mu_3\text{-}S)_8(PEt_3)_6]^+$ has been successfully isolated by reacting $[Fe(H_2O)_6]^{2+}$ with H_2S in the presence of PEt_3 and $[NBu^n{}_4][PF_6]$ with rigorous exclusion of oxygen and its molecular structure established by a single-crystal *X*-ray diffraction study [crystal data: trigonal, space group $R\bar{3}$, with a = 11.705(7) Å, α = 92.17(8)°, and Z = 1]. The structure was solved by the heavy-atom method and refined by full-matrix least-squares methods to a conventional R value of 0.054 for 1 146 observed reflections. The monopositive species, which is paramagnetic with a magnetic moment of 7.4 μ_B, is isostructural with the previously reported dication, its inner core consisting of an octahedron of iron atoms with all the faces symmetrically capped by sulphur ligands. The addition of one electron with respect to the dipositive species induces small changes in the metal framework.

Part of the proteins present in both lower and higher organisms are non-haem iron proteins, containing iron–sulphur clusters connected to the apoprotein through the side chains of cysteine amino acids. One of the major biological functions of these proteins is that of electron transport.[1] It is hence obvious that the evaluation of any molecule as a model of a biological redox site requires primarily the knowledge of its redox potential and its ability to undergo electron-transfer processes.

Since the pioneering work of Balch[2] on the Fe_4S_4 core, the electrochemistry of a wide range of iron–sulphur cores has been investigated: Fe_2S_2,[3–8] Fe_3S,[9] Fe_3S_4,[7] Fe_4S_2,[10] Fe_4S_4,[4,5,10–19] Fe_4S_5,[6] Fe_4S_6,[6] Fe_6S_6,[20–22] and Fe_6S_9.[7,23,24]

Biologically significant polynuclear Fe–S assemblies are actually restricted to Fe_2S_2, Fe_3S_3, and Fe_4S_4 cores;[1] however, recently interest has been directed towards 'non-conventional' cluster core structural types, which, stabilized by the protein environment, may be candidates for hitherto unrecognised redox sites in iron–sulphur proteins. On the other hand, the fundamental goal of the modelling strategy should be the laboratory reproduction of the dynamic functions of a biological substrate rather than the building of a static image. Therefore it was of interest to study the redox chemistry of the octahedral face-capped cluster $[Fe_6(\mu_3\text{-}S)_8(PEt_3)_6]^{2+}$, which has a large paramagnetism (six unpaired electrons per cluster unit), and is a suitable potential agent for multielectron transport processes.[25] The Fe_6S_8 core unit has been found to show an unusual ability to undergo reversible one-electron charge transfers. The new monopositive species $[Fe_6(\mu_3\text{-}S)_8(PEt_3)_6]^+$ has been isolated and structurally characterized.

Table 1. Crystal data and data collection details

Formula	$C_{36}H_{90}F_6Fe_6P_7S_8$
M	1 445.52
a/Å	11.705(7)
α/°	92.17(8)
D_c/g cm^{-3}	1.500
U/Å^3	1 600.1
Z	1
Space group	$R\bar{3}$
μ(Mo-K_α)/cm^{-1}	17.91
Transmission factors	0.75—0.82
Colour	black
Habit	regular prism
Dimensions (mm)	0.060 × 0.165 × 0.175
T/K	295
Radiation	Mo-K_α (λ = 0.7107 Å)
Monochromator	graphite crystal
Scan type	ω—2θ
Scan speed (° s^{-1})	0.06
Scan width (°)	0.7 + 0.3 tanθ
Background time	half the scan time
Standards	3 every 120 readings
Maximum deviation of standards (%)	2
2θ limits (°)	5—50
Data collected	$\pm h$, $\pm k$, $\pm l$, ($h \geqslant k \geqslant l$)
Total data	2 089
Data used [$I > 3\sigma(I)$]	1 146
Final variables	76
R, R'	0.054, 0.053

Experimental

Electrochemistry.—Acetonitrile and dichloromethane solvents (Burdick and Jackson, distilled in glass, u.v. grade) were used as received. Tetraethylammonium perchlorate (Carlo Erba) and tetrabutylammonium perchlorate (Fluka) supporting electrolytes were dried in a vacuum oven and used without

---

† Octa-μ_3-sulphido-hexakis(triethylphosphine)-*octahedro*-hexairon-(1+) hexafluorophosphate.

Supplementary data available: see Instructions for Authors, *J. Chem. Soc., Dalton Trans.*, 1987, Issue 1, pp. xvii—xx.

Non-S.I. unit employed: eV ≈ 1.60 × 10^{-19} J.

Table 2. Atomic co-ordinates (× 10^4)

Atom	*x*	*y*	*z*
Fe	915(1)	1 217(1)	−475(1)
S(1)	1 407(2)	1 407(2)	1 407(2)
S(2)	−655(2)	2 208(2)	−138(2)
P(1)	2 064(2)	2 638(2)	−1 107(2)
C(1)	3 497(7)	2 691(8)	−481(8)
C(2)	4 332(10)	3 645(10)	−872(10)
C(3)	2 258(8)	2 622(8)	−2 646(8)
C(4)	2 822(10)	1 580(9)	−3 149(9)
C(5)	1 568(9)	4 068(8)	−855(8)
C(6)	1 574(10)	4 490(10)	372(9)
P(2)	3 835(12)	3 835(12)	3 835(12)
F(1)	4 157(18)	2 574(19)	3 986(18)
F(2)	4 993(26)	3 859(30)	3 814(28)

purification. Deaeration of solutions was performed using ultra-pure nitrogen.

Electrochemical techniques were carried out using a PAR model 170 Electrochemistry System as polarizing unit; the recording device for potential scan rates higher than 0.5 V s^{-1} was a Hewlett-Packard model 1123 A storage oscilloscope.

Cyclic voltammetry was performed in a three-electrode cell having a platinum working electrode surrounded by a platinum-spiral counter electrode, and the reference electrode mounted with a Luggin capillary.

Controlled-potential coulometric tests were performed in a H-shaped cell with anodic and cathodic compartments separated by a sintered glass disc. The working macroelectrode was a platinum gauze; a mercury pool was used as counter electrode. In these tests an Amel potentiostat model 551, with an associated coulometer (Amel integrator model 558), were used.

In all electrochemical tests an aqueous saturated calomel electrode (s.c.e.) was used as reference electrode; the temperature was controlled at 20 ± 0.1 °C.

Synthesis of $[Fe_6(\mu_3\text{-}S)_8(PEt_3)_6][PF_6]$.—$[Fe(H_2O)_6][BF_4]_2$ (0.68 g, 2 mmol) and PEt_3 (0.71 g, 6 mmol) were dissolved in ethanol–methylene chloride (1:1, 50 cm^3). The H_2S was bubbled through for 5 min at room temperature. The resulting dark greenish solution was filtered and $[NBu^n{}_4][PF_6]$ (0.77 g, 2 mmol) was added. By evaporation of the solvent in a current of nitrogen, black crystals precipitated. These were recrystallized from methylene chloride–butanol. Yield: 15%, based on $[Fe(H_2O)_6][BF_4]_2$ (Found: C, 29.45; H, 6.20; Fe, 22.75. Calc. for $C_{36}H_{90}F_6Fe_6P_7S_8$: C, 29.9; H, 6.25; Fe, 23.2%).

Crystal Data and X-Ray Data Collection.—A black, well-formed crystal of approximate dimensions 0.175 × 0.165 × 0.060 mm was mounted along its crystallographic *b* axis on a Philips PW 1100 automatic four-circle diffractometer. Unit-cell dimensions were determined by a least-squares refinement of the setting angles of 20 carefully centred reflections. Crystal data and data collection details are given in Table 1. Intensity data were processed as described elsewhere.[26] The standard deviations $\sigma(I)$ of the intensity I were calculated, assigning a value of 0.03 for the instability factor k.[27] The intensities, after correction for background, were corrected for Lorentz-polarization effects. An absorption correction was applied, the range of transmission factors being 0.75—0.82.

Structure Solution and Refinement.—All the calculations were performed by using the SHELX 76[28] and ORTEP[29] programs on a SEL 32/77 computer. Atomic scattering factors were taken from ref. 30 for non-hydrogen atoms and from ref. 31 for the hydrogen atoms. Both the $\Delta f'$ and $\Delta f''$ components of the anomalous dispersion were included for the non-hydrogen atoms.[32] The function minimized during the least-squares refinement was $\Sigma w(|F_o| - |F_c|)^2$, the weights being defined as $w = 1/\sigma^2(F_o)$. The structure was solved by the heavy-atom method. The refinement was carried out by full-matrix least-squares techniques, assigning anisotropic thermal parameters to iron, sulphur, and phosphorus atoms. The hydrogen atoms were introduced in their geometrical positions, but were not refined. The hexafluorophosphate anion, being in the proximity of the inversion centre, could not be allowed a population parameter larger than 0.5. The refinement converged at the discrepancy indices R and R' of 0.054 and 0.053 respectively. Final atomic co-ordinates are given in Table 2.

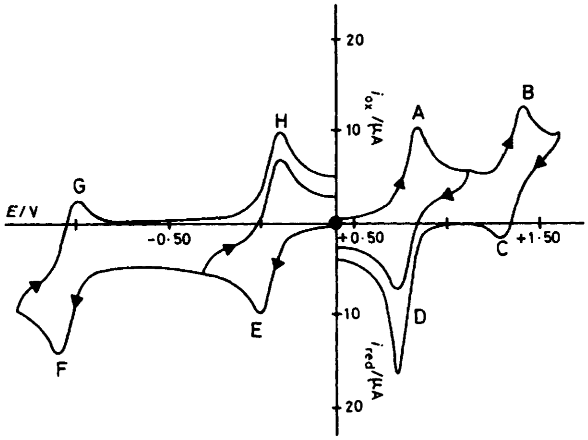

Figure 1. Cyclic voltammetric response recorded in a CH_2Cl_2 solution containing $[Fe_6S_8(PEt_3)_6][PF_6]_2$ (5.6 × 10^{-4} mol dm^{-3}) and $[NBu^n{}_4][ClO_4]$ (0.1 mol dm^{-3}). Platinum working electrode; scan rate 0.2 V s^{-1}; (●) starting potential

Results and Discussion

Electrochemistry.—The cyclic voltammogram obtained from a CH_2Cl_2 solution of $[Fe_6S_8(PEt_3)_6][PF_6]_2$* is reported in Figure 1. Two anodic and two cathodic processes are displayed. Controlled-potential coulometric experiments on both the first oxidation process, occurring at peak A, and the first reduction process, occurring at peak E, showed each of them to be due to a one-electron step. Hence, on the basis of their peak heights, the steps occurring at peaks B and F also involve one-electron charge transfers.

Cyclic voltammetry at scan rates (v) varying from 0.02 to 50 V s^{-1} shows the following features for the peak system A/D: the ratio $i_p(D)/i_p(A)$ is constantly equal to unity; the term $i_p(A)v^{-\frac{1}{2}}$ remains substantially constant; the parameter $\Delta E_p[= E_p(A) - E_p(D)]$ gradually increases from 68 mV at 0.02 V s^{-1} to 600 mV at 50 V s^{-1}. These data are diagnostic for an uncomplicated one-electron quasi-reversible charge transfer leading the $[Fe_6S_8]^{2+}$ core to the $[Fe_6S_8]^{3+}$ form, probably without gross changes in the molecular framework (+2/+3 redox change). Cyclic voltammetry on solutions exhaustively electrolyzed at +0.90 V confirms this datum; in fact it reveals the presence of the oxidized form of the +2/+3 couple.

The same diagnostic parameters for a quasi-reversible one-electron charge transfer hold as regards the peak system E/H, indicating that the starting $[Fe_6S_8]^{2+}$ unit can be electro-reduced to the $[Fe_6S_8]^{+}$ stable form. Also in this case cyclic voltammetry on solutions exhaustively electrolyzed at −0.30 V shows the presence of the reduced form of the +2/+1 couple.

Figure 1 shows that the anodic process occurring at peak B is

---

* This compound was prepared as described for the tetraphenylborate derivative,[25] using $[NBu^n{}_4][PF_6]$ in place of $Na[BPh_4]$.

Table 3. Standard electrode potentials (*vs.* s.c.e.) for the one-electron redox changes in the core of some high-nuclearity iron–sulphur clusters

		Core redox changes								
Core	Compound	4+/3+	3+/2+	2+/1+	1+/0	0/1−	1−/2−	2−/3−	Solvent	Ref.
Fe_6S_6	$[Fe_6S_6Cl_6]^{3-}$	+0.24	−0.70						CH_2Cl_2	21
		+0.30*	−0.75						MeCN	
Fe_6S_6	$[Fe_6S_6(SC_6H_4Me\text{-}p)_6]^{3-}$	−0.16	−1.09*						CH_2Cl_2	21
		−0.22	−1.04						MeCN	
Fe_6S_6	$[Fe_6S_6(OC_6H_4Me\text{-}p)_6]^{3-}$	−0.19							CH_2Cl_2	
		−0.11*							MeCN	21
Fe_6S_6	$[Fe_6S_6(OC_6H_4Cl\text{-}p)_6]^{3-}$		−1.19	−1.73*	−1.99*				MeCN	22
			−1.12	−1.73*	−2.04*				MeCN	22
Fe_6S_8	$[Fe_6S_8(PEt_3)_6]^{2+}$	+1.25	+0.59	−0.06	−1.05*				MeCN	This work
		+1.36	+0.80	+0.06	−1.03				CH_2Cl_2	
Fe_6S_9	$[Fe_6S_9(SCH_2Ph)_2]^{4-}$					+0.35	−0.41	−0.66	MeCN	23
	$[Fe_6S_9(SBu^t)_2]^{4-}$						−0.63	−1.72	Me_2SO	24

* Peak potential value for irreversible process.

complicated by electrode surface phenomena, as revealed by the spiked rereduction peak D in the reverse scan. At scan rates lower than 0.1 V s^{-1} the directly associated peak C is lacking and the peak D is more and more spiked. On the contrary, the increase of the scan rate restores the cathodic to anodic current ratio to unity, with ΔE_p values increasing as in the previous steps. These data may be interpreted in terms of electrodeposition of the electrogenerated $[Fe_6S_8]^{4+}$ species, which is desorbed and rereduced at the potentials of peak D. Attempts to obtain $[Fe_6S_8]^{4+}$ as an electrode deposit by electrolysis at + 1.5 V failed because the current rapidly faded away, indicating strong electrode poisoning effects. Hence we can assume the 4+/3+ couple to live at least in the short times of cyclic voltammetry, and the relevant charge transfer to be due to a quasi-reversible step.

Finally the analysis of the cyclic voltammograms relevant to the peak system F/G reveals this cathodic step to be due to a quasi-reversible one-electron charge transfer complicated by following chemical reactions. Controlled-potential coulometric experiments at −1.3 V showed the current to fall after the comsumption of 2 mol of electrons per mol of the starting derivative, but it remains higher than the current background even after the consumption of 3 mol of electrons. These data indicate that the electrogenerated $[Fe_6S_8]^0$ core is not stable over the long times of the electrolysis experiment, and it tends to decompose.

In summary, the iron–sulphur cluster investigated here exhibits the five-membered electron transfer series (1) in which

$$[Fe_6S_8]^{4+} \underset{-e^-}{\overset{+e^-}{\rightleftharpoons}} [Fe_6S_8]^{3+} \underset{-e^-}{\overset{+e^-}{\rightleftharpoons}} [Fe_6S_8]^{2+} \underset{-e^-}{\overset{+e^-}{\rightleftharpoons}} [Fe_6S_8]^{+} \underset{-e^-}{\overset{+e^-}{\rightleftharpoons}} [Fe_6S_8]^{0} \quad (1)$$

only the $[Fe_6S_8]^{4+}$ and $[Fe_6S_8]^0$ species are short-lived.

The same electrode behaviour has been observed in MeCN solvent; the only differences being that the 1+/2+, 2+/3+, and 3+/4+ redox changes are characterized by a greater degree of reversibility than in CH_2Cl_2, and the neutral species $[Fe_6S_8(PEt_3)_6]$ is adsorbed on the electrode surface. In addition, both the monopositive and the tripositive species slowly decompose in MeCN after a long time (1—3 h) of macroelectrolysis.

Table 3 summarizes the standard potentials of the redox changes described above, together with relevant data for high-nuclearity iron–sulphur clusters reported to date. It can be seen that the present Fe_6S_8 assembly is the most effective in undergoing one-electron transfer sequences leaving intact the iron–sulphur cluster system. Only in the case of the Fe_4S_4 core present in $[Fe_4(\mu_3\text{-}S)_4(\eta^5\text{-}C_5H_5)_4]$ has a similar remarkable electron-transfer ability been demonstrated.[13] This testifies to the flexibility of the $[Fe_6S_8]^{2+}$ geometry which is able to support both the core expansion accompanying reductions and the core contraction accompanying oxidations. In this connection Figure 2 reports a comparison of the electrochemical behaviour of $[Co_6S_8(PEt_3)_6]^+$ with that of $[Fe_6S_8(PEt_3)_6]^{2+}$ in CH_2Cl_2. Extensive redox behaviour is displayed; in fact the Co_6S_8 core can assume reversibly charges of 0, + 1, + 2, and + 3.[33]

These examples demonstrate the great ability of these types of clusters to act as reagents for multiple discrete one-electron, chemically reversible, charge transfers.

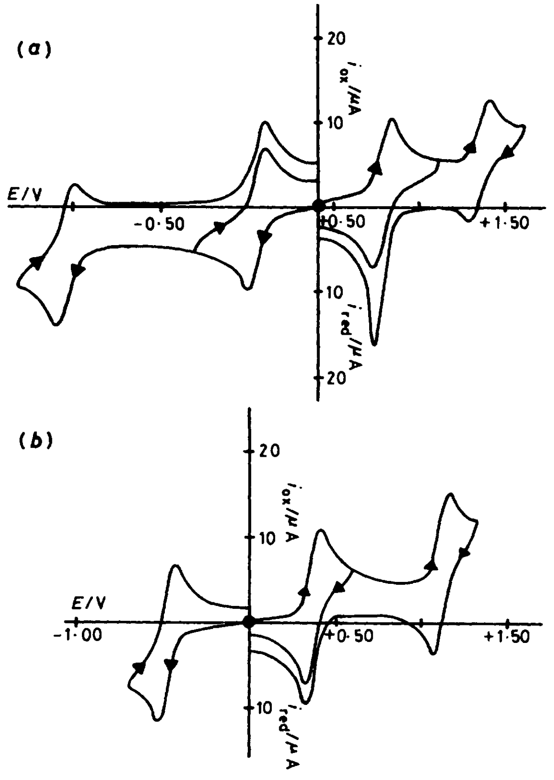

Figure 2. Cyclic voltammograms recorded in CH_2Cl_2 solutions containing $[NBu^n_4][ClO_4]$ (0.1 mol dm^{-3}) and (*a*) $[Fe_6S_8(PEt_3)_6][PF_6]_2$ (5.6 × 10^{-4} mol dm^{-3}) or (*b*) $[Co_6S_8(PEt_3)_6][PF_6]$ (6.9 × 10^{-4} mol dm^{-3}). Platinum working electrode; scan rate 0.2 V s^{-1}; (●) starting potential

Standard electrode potentials for electroactive species are usually related to the energies of the highest occupied and lowest unoccupied orbitals.[34] However, in the present case, such a relationship is not straightforward; SCF MS-X_α calculations for the dication[25] have shown a very crowded distribution of one-electron orbitals around 7 eV, which are partially occupied. Accordingly interelectronic repulsion should constitute the mean contribution to account for the experimental value of 0.6—0.7 eV calculated from the 3+/2+ and 2+/1+ redox potentials, and the contributions due to the solvation energies of the two redox species.

Synthesis and X-*Ray Structure of* $[Fe_6(\mu_3\text{-}S)_8(PEt_3)_6][PF_6]$.—The above electrochemical results showing the stability of the cations $[Fe_6(\mu_3\text{-}S)_8(PEt_3)]^+$ and $[Fe_6(\mu_3\text{-}S)_8(PEt_3)]^{3+}$ prompted us to attempt to isolate these new species.

The preparation of the monopositive and tripositive species was attempted by controlled-potential electrogeneration at a platinum macroelectrode. Unfortunately in CH_2Cl_2 solution these stable cationic species could not be separated using tetra-alkylammonium supporting electrolytes; on the contrary, in MeCN solution slow decomposition occurred. However, chemical reduction with sodium dihydronaphthylide or sodium tetrahydroborate afforded unidentified products, which in the light of the above electrochemical picture are probably mixtures of reduced forms of the starting dication, probably also with decomposition products.

The monopositive cation can be easily synthesized, however, by reacting $[Fe(H_2O)_6]^{2+}$ with H_2S in the presence of PEt_3 and $[NBu^n{}_4][PF_6]$, with rigorous exclusion of oxygen, equation (2).

$$[Fe(H_2O)_6]^{2+} \xrightarrow{PEt_3,\ H_2S} \underset{(\mathbf{1})}{[Fe_6(\mu_3\text{-}S)_8(PEt_3)_6]^+} \xrightarrow{O_2} \underset{(\mathbf{2})}{[Fe_6(\mu_3\text{-}S)_8(PEt_3)_6]^{2+}} \quad (2)$$

The solution of (**1**) is quickly oxidized by atmospheric oxygen, without apparent colour change, to yield the dipositive, previously reported, cation $[Fe_6(\mu_3\text{-}S)_8(PEt_3)_6]^{2+}$, (**2**). The solid complex is slowly oxidized in air.

Complex (**1**) is soluble in common polar organic solvents (*e.g.* nitroethane) in which it behaves as 1:1 electrolyte. The cluster is paramagnetic with an effective magnetic moment at room temperature of 7.4 μ_B. This value, which appears indicative of seven unpaired electrons, is in agreement with the 'quasi-atomic' model which provides seven and six unpaired electrons for (**1**) and (**2**) respectively.[25b,35]

Since the knowledge of the relationships between the structural parameters and the electron count is a key factor in understanding the rates and mechanism of charge-transfer reactions, we have carried out the crystal structure determination of the monopositive cation (**1**), which contains 91 valence electrons. The previously investigated clusters $[M_6(\mu_3\text{-}S)_8(PEt_3)_6]^{n+}$ (M = Fe, n = 2;[25] M = Co, n = 1 or 0[33]) are all isostructural their primary geometry remaining practically unchanged when the number of valence electrons varies from 90 to 97 and 98. However, on augmenting the number of valence electrons the metal-metal separation increases from 2.617(6) to 2.794(3) and 2.817(3) Å respectively.

The molecular structure of (**1**) consists of discrete $[Fe_6(\mu_3\text{-}S)_8(PEt_3)_6]^+$ cations and PF_6^- anions. A perspective view of the cation is shown in Figure 3; selected bond distances and angles are given in Table 4.

Table 4. Selected bond distances (Å) and angles (°) with estimated standard deviations in parentheses

Fe–Fe^a	2.636(2)	Fe–Fe^b	2.636(2)
Fe–S(1)	2.256(3)	Fe–S(2)^b	2.255(3)
Fe–S(2)	2.250(3)	Fe–S(2)^d	2.243(3)
mean Fe–S	2.251(3)*		
Fe–P(1)	2.263(3)		
Fe^a–Fe–Fe^b	90.0	Fe^a–Fe–Fe^c	60.0(1)
Fe^a–Fe–Fe^d	60.0	Fe^b–Fe–Fe^c	60.0(1)
S(1)–Fe–S(2)	88.8(1)	S(2)^b–Fe–S(2)^d	89.3(1)
S(1)–Fe–S(2)^d	89.0(1)	P(1)–Fe–S(1)	98.6(1)
S(1)–Fe–S(2)^b	165.4(1)	P(1)–Fe–S(2)	99.5(1)
S(2)–Fe–S(2)^d	165.5(1)	P(1)–Fe–S(2)^d	95.0(1)
S(2)–Fe–S(2)^b	89.2(1)	P(1)–Fe–S(2)^b	96.1(1)
Fe–S(1)–Fe^a	71.5(1)	Fe–S(2)–Fe^c	71.6(1)
Fe–S(2)–Fe^a	71.8(1)	Fe^a–S(2)–Fe^c	71.8(1)

Subscripts refer to the following equivalent positions: (a) z,x,y; (b) $\bar{z},\bar{x},\bar{y}$; (c) $\bar{y},\bar{z},\bar{x}$; (d) y,z,x.

* The estimated error on the mean was calculated according to the formula $[\Sigma_n(d_n - d)^2/n(n-1)]^{\frac{1}{2}}$.

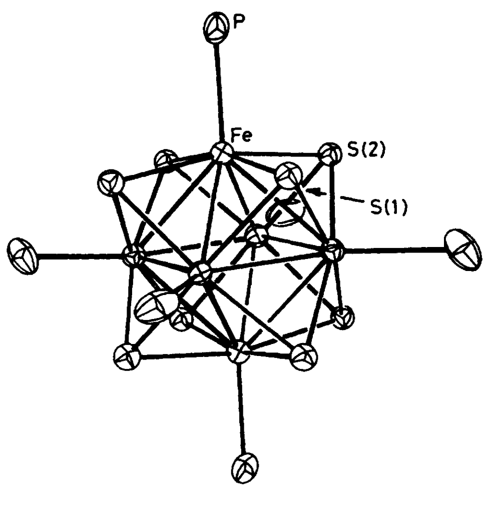

Figure 3. Inner core of the cluster cation $[Fe_6(\mu_3\text{-}S)_8(PEt_3)_6]^+$: ORTEP drawing with 30% probability ellipsoids

The cation, which is isostructural with the $[Fe_6(\mu_3\text{-}S)_8(PEt_3)_6]^{2+}$ dication, is built up of an octahedral cluster of iron atoms with all the faces symmetrically capped by triply bridging sulphur ligands. Moreover each metal atom is linked to a triethylphosphine group. The crystallographic symmetry is C_{3i} but the inner core, as shown by the values of the bond lengths and angles, may be considered to possess O_h symmetry. The addition of one electron, leaving unchanged the metal framework, induces an elongation of the metal–metal distances whose mean value is 2.617(6) Å in (**2**) and 2.636(2) Å in (**1**). This difference, although small, is of the same order that we have found between $[Co_6(\mu_3\text{-}S)_8(PEt_3)_6]^+$ and $[Co_6(\mu_3\text{-}S)_8(PEt_3)_6]$[33] and larger than those found for instance for the clusters $[Co_8S_6(SPh)_6]^{4-,5-}$[36] and $[Fe_6S_6Cl_6]^{2-,3-}$.[37] Moreover while the Fe–P distance of 2.263(3) Å in (**1**) is shorter than the value of 2.293(6) Å in (**2**), the Fe–S distances in the two clusters do not vary significantly. The above variations in the structural parameters follow the previously described[33c] trend observed for the species with 90, 97, and 98 electrons, providing further evidence for the great flexibility of the M_6S_8 core, which functions as an efficient electron reservoir.

Acknowledgements

We wish to thank Mr. F. Nuzzi for the microanalyses.

References

1 J. M. Berg and R. H. Holm, in 'Iron-Sulfur Proteins,' ed. T. G. Spiro, Wiley, New York, 1982, vol. 4.
2 A. L. Balch, *J. Am. Chem. Soc.*, 1969, **91**, 6962.
3 J. J. Mayerle, S. E. Denmark, B. V. De Pamphilis, J. A. Ibers, and R. H. Holm, *J. Am. Chem. Soc.*, 1975, **97**, 1032.
4 J. Cambray, R. W. Laue, A. G. Wedd, R. W. Johnson, and R. H. Holm, *Inorg. Chem.*, 1977, **16**, 2565.
5 G. B. Wong, M. A. Bobrik, and R. H. Holm, *Inorg. Chem.*, 1978, **17**, 578.
6 G. J. Kubas and P. J. Vergamini, *Inorg. Chem.*, 1981, **20**, 2667.
7 K. J. Hagen, A. D. Watson, and R. H. Holm, *J. Am. Chem. Soc.*, 1983, **105**, 3905.
8 W. E. Cleland, jun., and B. A. Averill, *Inorg. Chem.*, 1984, **23**, 4192.
9 K. S. Hagen, G. Christou, and R. H. Holm, *Inorg. Chem.*, 1983, **22**, 309.
10 R. S. Gall, C. T-W. Chu, and L. F. Dahl, *J. Am. Chem. Soc.*, 1974, **96**, 4019.
11 J. A. Ferguson and T. J. Meyer, *Chem. Commun.*, 1971, 623.
12 B. V. De Pamphilis, B. A. Averill, T. Herskovitz, L. Que, jun., and R. H. Holm, *J. Am. Chem. Soc.*, 1974, **96**, 4159.
13 Trinh-Toan, B. K. Teo, J. A. Ferguson, T. J. Meyer, and L. F. Dahl, *J. Am. Chem. Soc.*, 1977, **99**, 408.
14 R. W. Johnson and R. H. Holm, *J. Am. Chem. Soc.*, 1978, **100**, 5338.
15 P. K. Masharak, K. S. Hagen, J. T. Spence, and R. H. Holm, *Inorg. Chim. Acta*, 1983, **80**, 157.
16 W. E. Cleland, D. A. Holtman, M. Sabat, J. A. Ibers, G. C. De Fotis, and B. A. Averill, *J. Am. Chem. Soc.*, 1983, **105**, 6021.
17 M. G. Kanatzidis, N. C. Baenziger, D. Coucovanis, A. Simopoulos, and A. Kostikas, *J. Am. Chem. Soc.*, 1984, **106**, 4500.
18 T. O'Sullivan and M. Millar, *J. Am. Chem. Soc.*, 1985, **107**, 4096.
19 T. J. Ollerenshaw, C. D. Garner, B. Odell, and W. Clegg, *J. Chem. Soc., Dalton Trans.*, 1985, 2161.
20 D. Coucovanis, M. G. Kanatzidis, W. R. Dunham, and W. R. Hagen, *J. Am. Chem. Soc.*, 1984, **106**, 7998.
21 M. G. Kanatzidis, W. R. Hagen, W. R. Dunham, R. K. Lester, and D. Coucovanis, *J. Am. Chem. Soc.*, 1985, **107**, 953.
22 W. E. Cleland, jun., and B. A. Averill, *Inorg. Chim. Acta*, 1985, **106**, L17.
23 G. Henkel, H. Strasdeit, and B. Krebs, *Angew. Chem., Int. Ed. Engl.*, 1982 **21**, 201.
24 G. Christou, M. Sabat, J. A. Ibers, and R. H. Holm, *Inorg. Chem.*, 1982, **21**, 3518.
25 (*a*) F. Cecconi, C. A. Ghilardi, and S. Midollini, *J. Chem. Soc., Chem. Commun.*, 1981, 640; (*b*) A. Agresti, M. Bacci, F. Cecconi, C. A. Ghilardi, and S. Midollini, *Inorg. Chem.*, 1985, **24**, 689.
26 A. Bianchi, P. Dapporto, G. Fallani, C. A. Ghilardi, and L. Sacconi, *J. Chem. Soc., Dalton Trans.*, 1973, 641.
27 P. W. R. Corfield, R. J. Doedens, and J. A. Ibers, *Inorg. Chem.*, 1967, **6**, 197.
28 G. M. Sheldrick, SHELX System of Computing Programs, University of Cambridge, 1976.
29 C. K. Johnson, ORTEP Report ORNL-5138, Oak Ridge National Laboratory, Tennessee, 1976.
30 'International Tables for *X*-Ray Crystallography,' Kynoch Press, Birmingham 1974, vol. 1, p. 99.
31 R. F. Stewart, E. R. Davidson, and W. T. Simpson, *J. Chem. Phys.*, 1965, **42**, 3175.
32 Ref. 30, p. 149.
33 (*a*) F. Cecconi, C. A. Ghilardi, and S. Midollini, *Inorg. Chim. Acta*, 1981, **64**, L4; (*b*) F. Cecconi, C. A. Ghilardi, S. Midollini, and A. Orlandini, *ibid.*, 1983, **76**, L183; (*c*) F. Cecconi, C. A. Ghilardi, S. Midollini, A. Orlandini, and P. Zanello, *Polyhedron*, in the press.
34 F. D. Saeva and G. R. Olin, *J. Am. Chem. Soc.*, 1980, **102**, 299.
35 M. Bacci, *Phys. Lett. A*, 1983, **99**, 230.
36 G. Christou, K. S. Hagen, I. K. Bashkin, and R. H. Holm, *Inorg. Chem.*, 1985, **24**, 1010.
37 D. Coucouvanis, M. G. Kanitzidis, W. R. Dunham, and W. R. Hagen, *J. Am. Chem. Soc.*, 1985, **106**, 2998.

Received 20*th March* 1986; *Paper* 6/547